8-1-2018

Recoil-ion detection efficiency for complex β decays studied using the Beta-decay Paul Trap

J. M. Munson
University of California, Berkeley

K. Siegl
University of Notre Dame

N. D. Scielzo
Lawrence Livermore National Laboratory

B. S. Alan
University of California, Berkeley

A. Czeszumska
University of California, Berkeley

See next page for additional authors

Recommended Citation

Munson, J., Siegl, K., Scielzo, N., Alan, B., Czeszumska, A., Savard, G., Aprahamian, A., Caldwell, S., Chiara, C., Clark, J., Greene, J., Harker, J., Marley, S., Morgan, G., Norman, E., Orford, R., Padgett, S., Galvan, A., Sharma, K., & Strauss, S. (2018). Recoil-ion detection efficiency for complex β decays studied using the Beta-decay Paul Trap. *Nuclear Instruments and Methods in Physics Research, Section A: Accelerators, Spectrometers, Detectors and Associated Equipment, 898*, 60-66. https://doi.org/10.1016/j.nima.2018.04.063

Nuclear Inst. and Methods in Physics Research, A 898 (2018) 60–66

Contents lists available at ScienceDirect

Nuclear Inst. and Methods in Physics Research, A

journal homepage: www.elsevier.com/locate/nima

Recoil-ion detection efficiency for complex β decays studied using the Beta-decay Paul Trap

J.M. Munson [a], K. Siegl [b,c], N.D. Scielzo [c,*], B.S. Alan [a,c], A. Czeszumska [a,c,1], G. Savard [d,e], A. Aprahamian [b], S.A. Caldwell [d,e,2], C.J. Chiara [d,f,3], J.A. Clark [d,i], J.P. Greene [d], J. Harker [f,d], S.T. Marley [b,g], G.E. Morgan [i,4], E.B. Norman [a,c], R. Orford [d,h], S.W. Padgett [c], A. Perez Galvan [d,5], K.S. Sharma [i], S.Y. Strauss [b]

[a] Department of Nuclear Engineering, University of California, Berkeley, CA 94720, USA
[b] Department of Physics, University of Notre Dame, Notre Dame, IN 46556, USA
[c] Nuclear and Chemical Sciences Division, Lawrence Livermore National Laboratory, Livermore, CA, 94550, USA
[d] Physics Division, Argonne National Laboratory, Argonne, IL 60439, USA
[e] Department of Physics, University of Chicago, Chicago, IL 60637, USA
[f] Department of Chemistry and Biochemistry, University of Maryland, College Park, MD 20742, USA
[g] Department of Physics and Astronomy, Louisiana State University, Baton Rouge, LA 70803, USA
[h] Department of Physics, McGill University, Montréal, Québec H3A 2T8, Canada
[i] Department of Physics and Astronomy, University of Manitoba, Winnipeg, Manitoba R3T 2N2, Canada

ARTICLE INFO

Keywords:
β-delayed neutron decay

ABSTRACT

Beta-delayed neutron emission is being studied by detecting the β particles and recoiling ions emerging from the Beta-decay Paul Trap. For β decays to the ground state or γ-emitting states of the daughter nucleus, the fraction of recoiling ions which reach the ion detector in coincidence with a β particle has been determined for ^{134,135}Sb, ^{137,138,140}I, and ^{144,145}Cs. This value is needed for the determination of the β-delayed neutron emission branching ratio solely from the recoil-ion time-of-flight (TOF) spectrum. The β-particle energy and recoil-ion TOF spectra were used to constrain a simple decay model, which can be used to determine the detection efficiency. The method is compared to simulations to estimate the uncertainty introduced by incomplete knowledge of the decay pattern. By fitting the simulation results to several β-ion coincidence properties measured during the experiment, the fraction of ions which reach the microchannel plate detector can be determined to within $\pm$4%. This result opens the possibility of using the recoil-ion TOF spectra for high precision β-delayed neutron branching-ratio measurements.

1. Introduction

Detailed studies of beta-delayed neutron (βn) emission are important for establishing a better understanding of the nuclear structure of neutron-rich nuclei, the production of heavy elements in the cosmos, and applications of nuclear science involved in nuclear-energy generation and national-security missions. Improved measurements of βn emission for fission products have the potential to reduce the conservative margin needed for the safe operation of nuclear reactors, resulting in reduced costs [1], and more precise nuclear reactor kinematic and dynamic calculations have made the βn energy spectrum increasingly important [2], particularly for fast reactors [3]. In addition, improved nuclear data for fission products would benefit the stockpile-stewardship and nuclear-forensics missions [1]. The isotopic abundance patterns for the elements heavier than iron produced in the astrophysical rapid neutron capture (r) process is influenced by βn emission by changing the mass flow during the decay back to stability and by providing a delayed population of neutrons for neutron-capture reactions [4].

The Beta-decay Paul Trap (BPT) was designed and built for detailed studies of β decay, and has been used to investigate βn emission [5–7].

* Corresponding author.
E-mail address: scielzo1@llnl.gov (N.D. Scielzo).
[1] Current address: Research Center for Nuclear Physics, Osaka University, Ibaraki, Osaka 567-0047, Japan.
[2] Current address: Rigetti Computing, 775 Heinz Avenue, Berkeley, CA 94606, USA.
[3] Current address: U.S. Army Research Laboratory, Adelphi, MD 20783, USA.
[4] Current Address: Department of Physics and Astronomy, Louisiana State University, Baton Rouge, LA 70803, USA.
[5] Current address: Vertex Pharmaceuticals, 11010 Torreyana Road, San Diego, CA 92121, USA.

https://doi.org/10.1016/j.nima.2018.04.063
Received 21 February 2018; Received in revised form 27 April 2018; Accepted 30 April 2018
Available online 7 May 2018
0168-9002/

The BPT is a radio-frequency quadrupole (RFQ) ion trap with an open electrode geometry that allowed a set of radiation detectors to surround the trapped-ion cloud [8]. The use of an RFQ trap in conjunction with microchannel plate (MCP) detectors allows the detection of the low-energy recoiling daughter nucleus following either β decay or βn emission. Plastic scintillator detectors were used to observe the coincident β particle and provide a start signal for the time-of-flight (TOF) of the daughter recoil ion. The emission of a neutron typically imparts larger recoil energies, which results in shorter TOFs for the recoiling ions. This allows the identification of βn events based on the TOF. As a result, the βn emission branching ratio, P_n, can be determined without the need for direct neutron detection by using the relation

$$P_n = \frac{N_{\beta R}}{N_{\beta R} + N_{\beta r}} = \frac{n_{\beta R}/\epsilon_{\beta R}}{n_{\beta R}/\epsilon_{\beta R} + n_{\beta r}/\epsilon_{\beta r}} = \frac{n_{\beta R}}{n_{\beta R} + n_{\beta r}\epsilon_{\beta R}/\epsilon_{\beta r}}. \quad (1)$$

Here $N_{\beta R}$, $n_{\beta R}$, and $\epsilon_{\beta R}$ are the number of βn decays, the number of detected β-ion coincidences from βn decay, and the efficiency for detecting these β-ion coincidences, respectively. $N_{\beta r}$, $n_{\beta r}$, and $\epsilon_{\beta r}$ refer to the same quantities but for β decays which do not subsequently result in neutron emission.

Although P_n can also be determined by comparing $n_{\beta R}$ to the number of detected β particles and the number of β-γ coincidences (as in Ref. [5]), a result obtained solely from β-ion coincidences using Eq. (1) has the advantage that it is a ratio involving the same detectors and coincidence requirements. Therefore, this measurement approach can potentially reach the highest precision if the ratio $\epsilon_{\beta R}/\epsilon_{\beta r}$ can be accurately determined.

In the ratio $\epsilon_{\beta R}/\epsilon_{\beta r}$, quantities such as the intrinsic efficiencies and solid angles of both the MCP detector and the β detector cancel out to a large degree. The β-particle detection efficiencies are nearly independent of the energy distribution because a low-energy threshold (70 keV) was used; the resulting small deviation from unity in the ratio due to threshold effects and scattering can be calculated with reasonable precision. The intrinsic efficiency for detecting the recoil ions striking the MCP detector is also nearly independent of the initial recoil energies because the ions are all accelerated to energies >5 keV, for which the intrinsic efficiency is nearly independent of impact energy [9]. This leaves the main challenge in determining the ratio $\epsilon_{\beta R}/\epsilon_{\beta r}$ as determining the fraction of ions which reach the MCP detector for the two decay modes.

The value of $\epsilon_{\beta R}$, although somewhat dependent on the neutron-energy distribution, is significantly more straightforward than $\epsilon_{\beta r}$ to determine. For all but the lowest-energy neutrons, the corresponding ion momentum is dominated by the recoil imparted by the emitted neutron, and the recoil energy is large enough that the ion trajectories are only minimally perturbed by the electric fields of the trap. In addition, the β decays to the neutron-unbound states are expected to be predominantly allowed in character, so the direction of the neutron and β-particle momenta are not expected to be correlated. As a result, the fraction of these ions reaching the MCP detector, and therefore $\epsilon_{\beta R}$, is largely dependent on detector solid angles.

For $\epsilon_{\beta r}$, the situation is not as simple. For decays without neutron emission, the recoil energies are all less than 400 eV and therefore the ion trajectories are significantly perturbed by the 200 V peak-to-peak RF voltage of the trap. The initial recoil momentum of the ions is also dependent on the β-ν angular-correlation coefficients ($a_{\beta\nu}$) of the transitions as well as the details of any subsequent cascade of γ rays and conversion electrons (CEs). For first-forbidden transitions, the values for $a_{\beta\nu}$ can depend on several β-decay matrix elements [10] and are typically difficult to predict. Therefore, determining the fraction of ions which reach the MCP detector is not straightforward.

This paper focuses on the development of a method for precisely determining the fraction of ions which reach the MCP detector, and therefore $\epsilon_{\beta r}$, despite the aforementioned challenges. A simple model that uses a set of fictitious β-decay branches and a single, average value for the β-ν angular correlation coefficient for all transitions is demonstrated to accurately determine the fraction of ions which reach the recoil-ion detector if the decay properties are adjusted to match certain key properties of the data. This approach depends only on data collected using the BPT and therefore can be used even in the complete absence of prior knowledge of the decay properties. This feature is important as the availability of reliable β-decay data varies considerably and is quite limited for most isotopes far from stability.

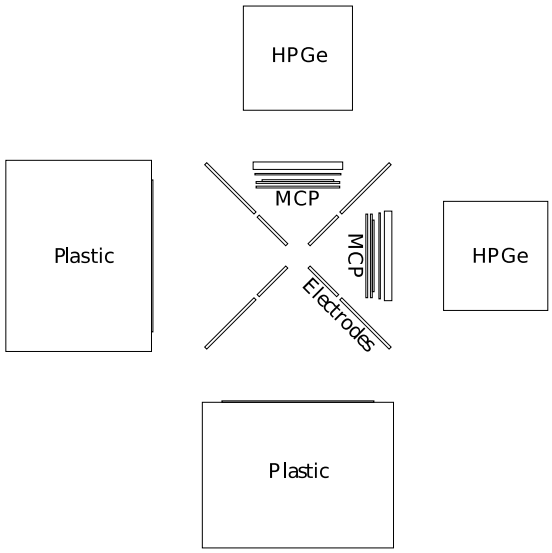

Fig. 1. The BPT and associated detectors, viewed along the beam axis. The beam axis points out of the page and the detectors are identified according to their positioning relative to the axis. In the left and bottom positions are the two ΔE–E plastic scintillator detectors used for β-particle detection, and in the right and top positions are two MCP detectors and two HPGe detectors used for recoil-ion and γ-ray detection, respectively.

2. Experiment

The β decays of ^{134,135}Sb, ^{137,138,140}I, and ^{144,145}Cs were studied using the BPT instrumented with a detector array consisting of two MCP detectors, two ΔE–E plastic scintillator telescopes, and two high-purity germanium (HPGe) detectors for the detection of recoil ions, β particles, and γ rays, respectively. The detector geometry is shown in Fig. 1. The focus of these experiments was to study βn emission properties by measuring the time-of-flight (TOF) of the recoiling daughter nuclei. This approach and the experimental system are described in detail in Refs. [5–7,11] so only a brief summary is provided here.

The ions were provided from the spontaneous fission of a ~100-mCi ^{252}Cf source at the Californium Rare Isotope Breeder Upgrade (CARIBU) [12] located at the Argonne Tandem Linac Accelerator System (ATLAS) facility at Argonne National Laboratory. The isotopes were delivered as singly-charged mass-separated ion beams with intensities which ranged from ~1000 ions/s (^{137}I) to ~10 ions/s (^{140}I). For ^{135}Sb, ^{138}I, and ^{144,145}Cs, the beams had a radiopurity of >95%. For the ^{134}Sb, ^{137}I and ^{140}I analysis, contributions from ^{134m}Sb, ^{137}Te and ^{140}Xe ions observed to be present in the trap, respectively, had to be identified based on the order-of-magnitude difference in the radioactive half-lives of the species involved. The mass selectivity of the ion delivery was not sufficient provide any suppression of ^{134}Sb from the high-spin ^{134m}Sb isomer. The ^{134}Sb contribution was isolated by taking the appropriate combination of data collected under two different measurement conditions [11].

The ions delivered to the BPT were confined radially by applying ≈200 V peak-to-peak RF voltage at 310 kHz to four sets of thin electrode

Table 1
The estimated average recoil-ion charge state and 180°/90° coincidence ratio determined from the data for each isotope.

Isotope	Average charge state	$R_{180/90}$
^{134}Sb	2.44	9.38 ± 0.68
^{135}Sb	2.20	5.85 ± 0.15
^{137}I	2.28	5.97 ± 0.20
^{138}I	2.25	3.08 ± 0.02
^{140}I	2.16	3.91 ± 0.22
^{144}Cs	2.45	3.33 ± 0.02
^{145}Cs	2.13	3.66 ± 0.05

plates which were positioned with the interior edge within 11 mm of the trap center. Each of the electrode plates was divided into three segments along the beam axis and the ions were confined axially by DC voltages of +20 V, −17 V, and +20 V applied on the segments. Manipulation of the DC offsets applied to the entrance and exit sections allowed ion loading and ejection. The trap volume was suffused with helium buffer gas at a pressure of $\sim 5 \times 10^{-5}$ Torr to cool the trapped ions and reduce the spatial extent of the ion cloud to ~1 mm^3.

The MCP detector assemblies consisted of two MCP plates arranged in a chevron configuration and backed by a resistive anode, and provide both sub-mm position and ~1-ns timing information for the recoiling ions. The detectors were located 53.0(5) mm from the center of the ion cloud and had a nominal sensitive area of 50 × 50 mm^2. Events which fell within a fiducial area of 46 × 46 mm^2, where hit locations could be precisely determined, were used in the analysis of the data. Grounded 89%-transmission screens were placed 4.5 mm in front of each MCP detector and a −2500 V bias was applied to the front face of the detectors to accelerate the ions for nearly uniform detection.

Each plastic-scintillator telescope consisted of a 1-mm-thick, 106.6-mm-diameter ΔE detector backed by a 102-mm-thick, 133-mm-diameter E detector. The E detector was coupled directly to a single 127-mm photomultiplier tube (PMT) while the ΔE detector was coupled to two 38.1-mm PMTs via a light-pipe structure. The small thickness of the ΔE detector minimized its sensitivity to γ rays, allowing the ΔE detector to be used to identify incoming β particles.

The recoil-ion TOF was determined from coincidences between a ΔE plastic detector and an MCP detector. The detectors are identified according to their positioning relative to the beam axis. In the left and bottom positions are the two ΔE–E plastic scintillator detectors, and in the right and top positions are two MCP detectors and two HPGe detectors. The ratio of the coincidences detected with the ΔE-MCP detector pair separated by 180°, $n_{\beta r}(180°)$, and the detector pairs separated by 90°, $n_{\beta r}(90°)$, denoted

$$R_{180/90} = \frac{n_{\beta r}(180°)}{n_{\beta r}(90°)}, \tag{2}$$

is found to be an important measured property that needs to be matched by the β-decay simulation. The experimental results for $R_{180/90}$ for all the isotopes studied here are given in Table 1.

The daughter ions charge-state distributions were inferred from the magnitude of the RF-phase dependence of the measured β-ion coincidence rates using the approach described in detail in Ref. [11]. A simple charge-state-distribution model including the 2^+, 3^+, and 4^+ ions was used where each charge-state abundance is reduced by a constant multiplicative factor (fit to best reproduce the RF-dependence of the data) from the one before it. The average charge state resulting from this simple model for each isotope is listed in Table 1.

3. Simulation

3.1. Decay properties

Simulations were used to generate β-decay distributions for a given β-ν correlation coefficient, set of β-decay feeding properties, and γ-ray decay scheme using an existing Monte-Carlo code for β decay [13], which includes $\beta\gamma$ and βn decay processes [6]. The β-decay transitions are all assumed to have an allowed energy distribution. The recoil-ion momenta are determined from conservation of momentum. The β-decay feeding and subsequent excited-state decay properties are provided by either data available in the Nuclear Data Sheets (NDS) [14–21], from measurements made using the Modular Total Absorption Spectrometer (MTAS) [22], or are considered unknown, in which case they must be adjusted such that the simulated plastic E detector energy spectra reproduce the experimental data. For the NDS and MTAS cases, the Reference Input Parameter Library (RIPL-3) [23] is used to describe the γ-ray cascade for each populated excited state. For the case where the β-decay feeding is considered unknown, fictitious excited states spaced at 1-MeV intervals in the daughter nucleus are used ("fictitious states model"), as shown in Fig. 2. In this case, the γ-ray cascade is constructed such that excited states up to a chosen maximum γ-ray energy deexcite to the ground state by emitting a single γ ray, while higher excited states emit a γ ray at this maximum energy (followed by additional γ-ray emission by the lower-energy states until the ground state is reached).

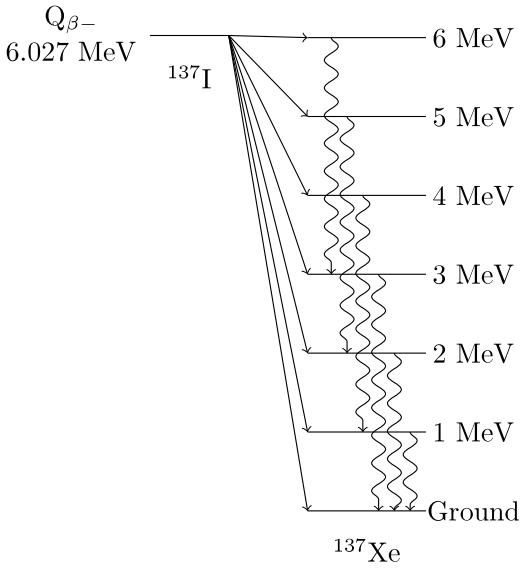

Fig. 2. Levels and decay scheme for the 3 MeV γ-ray fictitious states model.

The daughter ions are assigned a charge state of either 2^+, 3^+, or 4^+ with likelihoods based on the average charge state for each isotope listed in Table 1. The location of the decays within the ion cloud are distributed with a Gaussian distribution of 1 mm at FWHM (assumed to be identical in all three spatial dimensions).

3.2. Particle propagation

The recoil ions are then propagated through the time-varying electric-field environment of the BPT using the ion-optics program SimIon [24] to determine which ions strike an MCP detector. For each ion that hit an MCP detector, the TOF, hit position, impact energy, and RF phase at the time of the decay were recorded. Impacts located within a 46 × 46 mm^2 fiducial area on either MCP are accepted to match a corresponding cut used on the experimental data. A cut was applied to account for the fraction of MCP ion hits not recorded in the experiment due to the signal pulses falling below the electronic threshold [7]. In addition, the measured MCP intrinsic efficiencies of 33.3(15)% and 29.3(14)% for the right and top detectors, respectively, were used to adjust the simulated number of detected ions [11]. This factor accounts for ions that are lost to either one of the grids or to the inactive channel structure of the MCP detector as these losses are not otherwise included in the simulation.

The emitted β particle and any accompanying γ rays and CEs were propagated through a GEANT4 [25] simulation of the apparatus to identify decays which deposit energy in the ΔE and E plastic scintillators. For decays which deposit more than 70 keV in the ΔE detector, the timing and energies deposited in the plastic scintillators were recorded and convoluted with the energy resolution of these detectors.

The β-ion TOF coincidences were then identified from decays in which the detection requirements for both a ΔE and MCP detector were satisfied. This ΔE-MCP detector coincidence requirement ensures that all the detected particles originate from decays within the ion cloud. This energy spectrum differed from the true β-decay energy spectrum because of the coincidence requirement (which favors high-energy β particles), the energy lost by the β particles passing through the ΔE detector, the detector response function, and any true summing in the E detector from coincident γ rays. These effects are all included in the simulations.

3.3. Determination of average $a_{\beta\nu}$

The β-ν angular-correlation coefficients $a_{\beta\nu}$ have a strong effect on $R_{180/90}$. For the isotopes studied here, many of the transitions are first-forbidden and can potentially have any value of $a_{\beta\nu}$ between -1 and 1. None of these correlation coefficients are known so an approximation was made that all β-decay branches for a given isotope have the same (initially unknown) value of $a_{\beta\nu}$. This shared "average" value of $a_{\beta\nu}$ is notated here as $\langle a_{\beta\nu}\rangle$. For a fixed set of β-decay feeding and deexcitation properties, the value of $\langle a_{\beta\nu}\rangle$ was set to the value found to make $R_{180/90}$ from the simulation results reproduce the experimental value. While this is a somewhat coarse approximation, it is adequate for determining the singles and coincidence detection efficiencies. For example, the fictitious-states model simulation for ^{137}I was repeated using $a_{\beta\nu} = -1/3$ for transitions to excited states at or above 4 MeV, $a_{\beta\nu} = 1$ for transitions to ground and excited states at or below 2 MeV, and a value of $\langle a_{\beta\nu}\rangle = 0.4$ for the artificial state at 3 MeV, the value of which was selected to match $R_{180/90}$ to the data. The detection efficiencies obtained were within 1% of the values obtained when a single value of 0.63 for $a_{\beta\nu}$ was used for all transitions, as needed to match the measured value of $R_{180/90}$.

4. Results and discussion

4.1. ^{137}I benchmark cases

Of the isotopes studied, the β-decay branching ratios for ^{137}I are the most reliable as both high-statistics HPGe data [17] and total absorption spectroscopy data [22] exist. The results for ^{137}I are shown in Fig. 3 to demonstrate the process. Simulations using the β-decay feeding either from the NDS or from MTAS measurements coupled with γ-ray cascade properties from RIPL-3 were performed. MTAS β-decay feeding data are available for excitation-energy bins, and these bins were associated with daughter-nucleus states to utilize the results in the simulation. In some cases, a bin can be assigned to a particular state listed in RIPL-3 without ambiguity, however, in other cases bins may coincide with either multiple or no known daughter states. In the case where there is more than one possible state for a given bin, the branching ratio was divided among the possible states using the branching ratios from the NDS. For bins which do not correspond with a known state, an artificial state was added at the center of the bin and assumed to deexcite by a single γ-ray directly to the ground state. For the NDS-based and MTAS-based fits, the only free parameters are the value of $\langle a_{\beta\nu}\rangle$ used to match the measured $R_{180/90}$ and a normalization factor to match the total number of counts. The β energy and TOF results are shown in Fig. 3 and both simulations are found to agree well with the data.

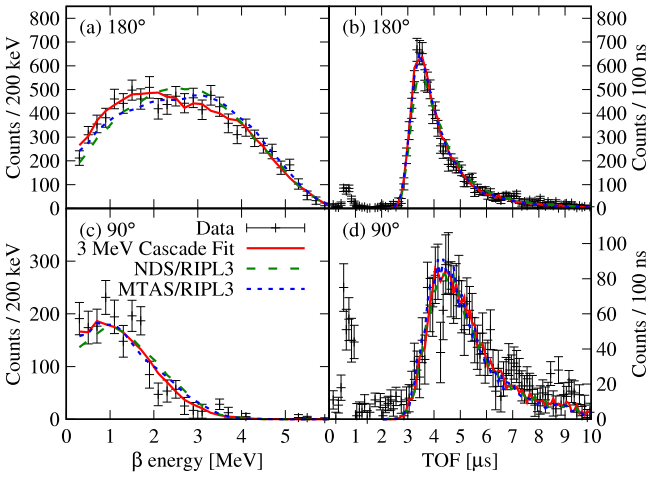

Fig. 3. (Color online) Comparison of the measured and simulated plastic E detector (β) spectra and the TOF spectra for ^{137}I β-ion coincidences. (a) The energy deposition in the E detector in coincidence with the opposite MCP detector (180° detector pairs), (b) the TOF for the 180° detector pairs, (c) the energy deposition in the E detector in coincidence with the adjacent MCP (90° detector pairs), (d) the TOF for the 90° detector pairs. The β-ion coincidences at TOFs less than 3 μs are from β-delayed neutron emission.

4.2. ^{137}I fictitious states model

The strength of the β-decay feeding to the states in the fictitious-states model was determined from the linear combination of simulated spectra which best reproduced the measured plastic detector energy spectra from the β-ion coincidence detected at 180°. This was accomplished by producing simulated spectra for β decays to the ground state and each excited state individually, with a common value for $\langle a_{\beta\nu}\rangle$, and then using a weighted sum to produce an overall spectrum for a given set of β-decay-feeding strengths. The resulting value of $R_{180/90}$ was determined and, if necessary, the value of $\langle a_{\beta\nu}\rangle$ was then adjusted and the process repeated until the $R_{180/90}$ in the simulation matched that of the data. This process was performed for models with different maximum γ-ray energies to investigate the sensitivity to the details of this simple model.

The choice of γ-ray cascade model affects the simulated value of $R_{180/90}$, and consequently affects the fitted value of $\langle a_{\beta\nu}\rangle$. For any excited state, deexcitation via a single γ ray to the ground state will result in larger average recoil energies than the isotropic emission of several lower energy γ rays. The additional recoil imparted from γ-ray emission affects the β-recoil angular distribution, shifting the value of $R_{180/90}$ closer to unity. To maintain the experimental value of $R_{180/90}$ in the simulation, the value of $\langle a_{\beta\nu}\rangle$ must be increased for γ-ray cascade models with a higher maximum γ-ray energy.

The γ-ray cascade model also affects the simulated TOF spectra. The cascades that involve higher-energy γ rays lead to more sharply-peaked TOF distributions, as can be seen in Fig. 4. The discrepancies between simulated and measured TOF spectra are used to exclude γ-ray cascade models which predicted a number of counts near the TOF peak which differed from the measured value by more than 1σ. For ^{137}I, the 1-MeV and 2-MeV cascades are excluded for this reason. The 4-MeV cascade could also be excluded, but has been retained to demonstrate how the cascade selection affects the results.

The predictive power of the fictitious-states model approach is examined in Fig. 5. The direct β-decay feeding for each energy bin determined using this model is compared to the results listed in the NDS and from a recent measurement using the MTAS. The fit results from the model reproduces the overall split between feeding to the ground state and excited states, although it produces a different distribution of feeding to the excited states. While this comparison shows limitations

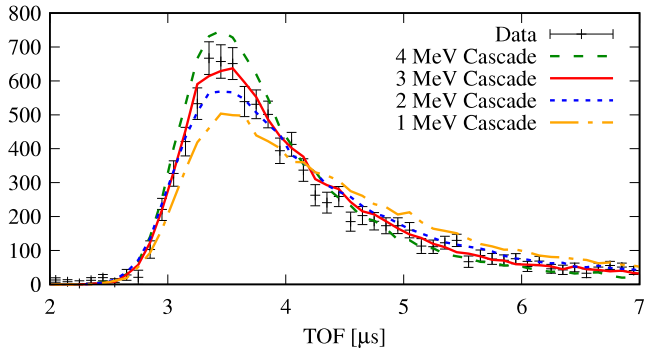

Fig. 4. (Color online) The measured recoil-ion TOF spectrum for ^{137}I compared to the simulation results obtained using different decay models. The TOF spectra resulting from the 1-MeV, 2-MeV, and 4-MeV γ-ray cascade models do not match the data well.

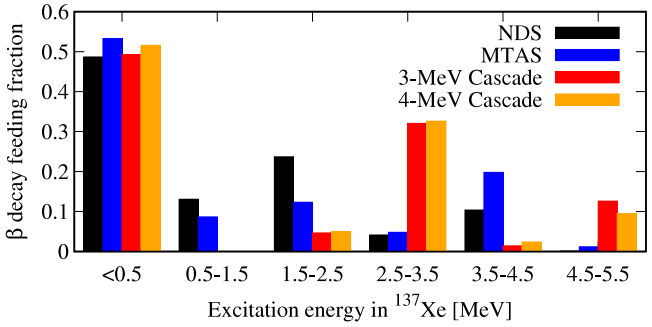

Fig. 5. (Color online) The β-decay feeding to 1-MeV excitation-energy bins in ^{137}Xe following the β decay of ^{137}I. The results of the γ-ray cascade models are compared to the nuclear data listed in the NDS [17] and recent MTAS [22] results.

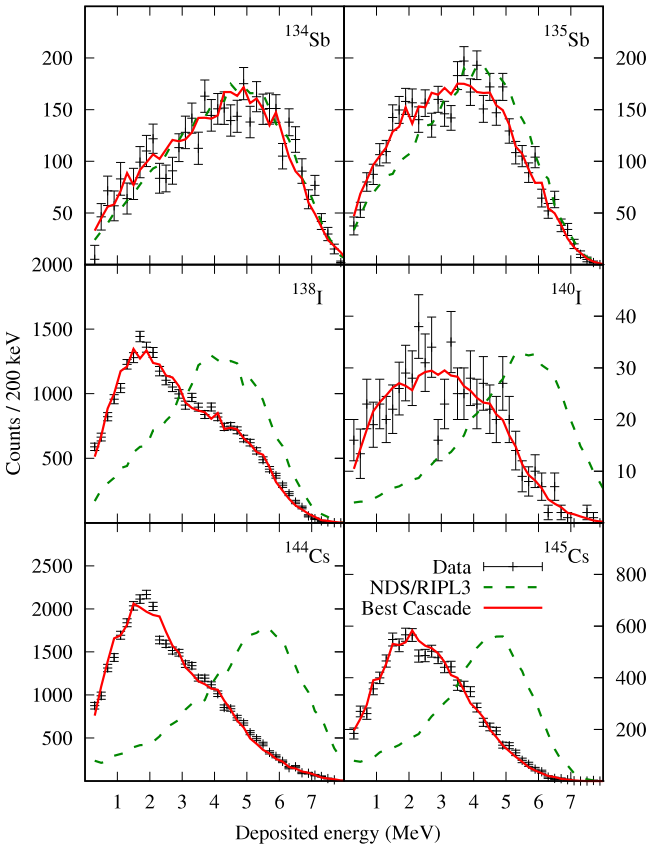

Fig. 6. (Color online) The β-energy spectra detected in the plastic E detector for β-ion coincidences in the 180° detector pairs. The results are compared to simulations using NDS/RIPL-3 input [14–21,23] along with fits using the γ-ray cascade models which best match the timing spectra for each isotope (see Section 4 for details).

in this approach, the general characteristics are reproduced sufficiently for the present purpose.

4.3. Other isotopes

The ^{134,135}Sb, ^{138,140}I, and ^{144,145}Cs β decays were analyzed using a similar approach and the results are shown in Fig. 6. The simulation for ^{134}Sb, which is dominated by the transition directly to the ground state, agrees relatively well with the measured data. In contrast, the energy spectra for the NDS/RIPL-3-based simulation results are weighted towards significantly higher energies than the data for the other cases, especially for ^{144,145}Cs and ^{138,140}I. These discrepancies are not completely unexpected given that these isotopes had only been previously studied using small-volume HPGe and Ge(Li) detectors [21,26], which give results susceptible to the "Pandemonium effect" [27]. This is a well-known problem that arises when the many β-decay transitions to higher excited states (which can sum together for a non-negligible combined strength) are misattributed to lower excited states due to their individual characteristic γ- ray signals being obscured in the detected γ-ray spectrum. For example, measured ^{145}Cs β-decay transitions which yield a daughter ^{145}Ba nucleus are only known to populate excited states up to 1.35 MeV [21], even though the β-decay Q value is 7.46 MeV. It is likely that there is additional β-decay strength populating states above 1.35 MeV of excitation energy. Measurements of β-particle energy spectra from Rudstam et al. [28] for these isotopes also indicate that there is additional feeding to higher-lying excited states.

Fig. 6 also depicts the results obtained from the fictitious-states model for each isotope. In each case, only the γ-ray cascade model which produced the closest match to the TOF spectra is shown. Using the fractions of decays directly feeding each fictitious state as free parameters allows the energy spectrum to be fit well to the data.

The β decays of ^{144}Cs and ^{145}Cs are accompanied by significant CE emission. Using the branching ratios from NDS [20,21] and cascade information from RIPL-3 [23], 6.2% of ^{144}Cs and 19.8% of ^{145}Cs β decays result in internal conversion. Internal conversion affects both the β- particle and the β-ion detection efficiencies by providing additional electrons that have enough energy to be detected in the ΔE detectors and by significantly increasing the charge state of the recoiling nuclei due to processes such as the emission of Auger electrons during the filling of inner-shell atomic vacancies [29]. The increased charge state of the recoiling ions causes the RF field to have a greater influence on their trajectories, which lowers the probability of reaching the MCP detectors. To account for these effects, the CE energies and intensities were included in the fictitious-states models to maintain the overall CE distribution present in the NDS/RIPL-3 simulations.

4.4. Efficiency results

A summary of the results for the efficiency of each detector and detector pair is shown in Table 2 for the various β-feeding and γ-ray cascade models. The detection efficiency of the right MCP detector is about 30% larger than the top MCP detector due to the lower gain of the top detector, which resulted in a larger number of ion hits falling below the electronic threshold [7], and the smaller intrinsic efficiency of the top detector found from the analysis of the ^{134}Sb data [11]. The MCP detectors and plastic-scintillator detectors subtend similar solid angles, but the MCP detection efficiency is significantly lower due to

Table 2
Detection efficiencies, average β-ν angular-correlation coefficients $\langle a_{\beta\nu}\rangle$, and average excitation energies $\langle E^*\rangle$ populated by the β-decay transitions for the various β-feeding and γ-ray cascade models for β decays without neutron emission. Intrinsic efficiency values of 29.3% and 33.3% for the top and right MCP detectors, respectively, determined in Ref. [11] are used. Values for $\langle a_{\beta\nu}\rangle$ which are outside the range −1 to 1 are not physical, however extrapolating is required to fit the experimental value for $R_{180/90}$ in these cases. If more than one fictitious-states cascade model produces acceptable TOF spectra, the closest match is indicated by *. The ^{144}Cs and ^{145}Cs fictitious-states models assume 6% and 20%, respectively, of the decays result in the emission of CEs (see Section 4 for details).

Isotope	Excitation and γ-ray cascade model	$\langle a_{\beta\nu}\rangle$	$\langle E^*\rangle$	MCP efficiency		Plastic efficiency		Coincidence efficiency			
			MeV	Top %	Right %	Left %	Bottom %	BT %	LR %	BR %	LT %
^{134}Sb	NDS/RIPL-3	0.48	0.07	1.10	1.44	6.65	6.79	0.347	0.451	0.048	0.037
	1 MeV	0.59	0.64	1.11	1.46	6.68	6.79	0.351	0.453	0.051	0.035
	2 MeV*	0.62	0.60	1.12	1.47	6.67	6.78	0.354	0.457	0.051	0.036
	3 MeV	0.66	0.63	1.12	1.48	6.66	6.78	0.355	0.458	0.051	0.036
^{135}Sb	NDS/RIPL-3	−0.27	1.01	1.01	1.35	6.68	6.83	0.256	0.330	0.058	0.043
	4 MeV	0.17	1.61	1.09	1.46	6.74	6.86	0.278	0.366	0.064	0.046
	5 MeV*	0.23	1.63	1.10	1.48	6.74	6.85	0.280	0.369	0.065	0.046
^{137}I	NDS/RIPL-3	0.11	1.15	0.97	1.30	6.70	6.79	0.236	0.308	0.053	0.038
	MTAS/RIPL-3	0.33	1.35	1.00	1.33	6.61	6.68	0.241	0.315	0.054	0.040
	3 MeV*	0.63	1.74	0.98	1.32	6.45	6.55	0.233	0.308	0.053	0.038
	4 MeV	0.65	1.63	1.00	1.35	6.50	6.60	0.239	0.317	0.055	0.039
^{138}I	NDS/RIPL-3	−1.24	1.22	0.98	1.33	6.81	6.95	0.170	0.228	0.074	0.053
	2 MeV	−0.93	3.09	0.96	1.29	6.78	6.90	0.162	0.214	0.071	0.052
	3 MeV*	−0.77	2.99	1.00	1.34	6.77	6.87	0.170	0.223	0.074	0.055
^{140}I	NDS/RIPL-3	−0.93	1.05	1.06	1.44	6.89	7.03	0.216	0.289	0.074	0.055
	2 MeV	−0.42	3.88	1.02	1.39	6.83	6.93	0.203	0.275	0.071	0.052
^{144}Cs	NDS/RIPL-3	−1.18	0.45	1.00	1.35	6.99	7.09	0.184	0.241	0.074	0.053
	3 MeV	−0.40	3.71	0.90	1.22	7.33	7.41	0.163	0.218	0.067	0.047
^{145}Cs	NDS/RIPL-3	−0.98	0.52	0.93	1.28	7.30	7.38	0.180	0.244	0.067	0.049
	3 MeV	−0.36	2.62	0.91	1.24	7.19	7.31	0.173	0.233	0.066	0.046

the intrinsic efficiency for recoil-ion detection and the impact of the RF electric field on the ion trajectories. The plastic detectors used to detect the β particles show little variation between isotopes since the β particles are generally well above the detection threshold. The slightly higher efficiency for the bottom detector as compared to the left detector is due to the bottom detector being approximately 1% closer to the trap center. The plastic detector efficiency is larger for the decays of ^{144}Cs and ^{145}Cs due to CE emission, which gives an additional electron with sufficient energy for detection.

The coincident β-ion efficiencies for 180° detector pairs are higher than for 90° pairs because the momentum imparted from β-particle emission causes the nucleus to recoil in the opposite direction. This effect is largest in ^{134}Sb, where a low average nuclear excitation following β decay results in fewer (isotropic) γ-ray emissions and therefore the β-particle momentum contributes a larger fraction of the total recoil. This effect also results in a correlation between results for $\langle E^*\rangle$ and $\langle a_{\beta\nu}\rangle$ — to maintain a fixed value for $R_{180/90}$, an increase in $\langle E^*\rangle$ requires an increase in $\langle a_{\beta\nu}\rangle$.

The overall systematic uncertainty in the determination of the β-ion coincidence efficiency that can be expected when using the evenly-spaced fictitious-states model was obtained by examining the ^{137}I results shown in Table 2. The results for the MCP, plastic detector, and β-ion efficiencies from the NDS-based and MTAS-based simulations agree with each other within about 3% and served as a benchmark against which the results of the fictitious-states model were compared. The results from the fictitious-states models using either the 3-MeV and 4-MeV γ-ray cascades all agree with the NDS-based and MTAS-based results, with the largest difference being 5%; the size of this difference was taken as a measure of the systematic uncertainty. A similar level of agreement is found for the decay of ^{134}Sb, although there the differences in the 90° detector pair shows a slightly larger variation.

A significant contributor to this uncertainty is the approximate treatment of the γ-decay cascade as can be seen in the variation between different cascade models for a given isotope.

Surprisingly, the efficiency values determined from the different models have such a small variation even in cases where there are large differences in the β-feeding distributions (as seen in the different energy spectra in Fig. 6 and the associated values of $\langle a_{\beta\nu}\rangle$). Here, it is evident that as long as the observed value of $R_{180/90}$ is reproduced by the β-decay properties in the simulation, the efficiency for detecting the recoil ions will remain largely unchanged. For all the cases other than ^{137}I, the decay properties obtained from the data collected in this work are taken to be the most reliable. As established with the ^{137}I results, the fictitious-states model correctly reproduces the gross features of the decay pattern and can determine the detection efficiency values to within ±4%. This level of precision paves the way for high precision β-delayed neutron emission branching ratio measurements using the recoil ion approach.

5. Conclusion

The fraction of recoil ions which reach an MCP detector following the β decay of isotopes held in the BPT is needed to determine β-delayed neutron emission branching ratios solely from β-ion coincidences. However, the existing information on the β-decay schemes for most isotopes is limited and properties such as β-ν angular correlations needed for detailed simulations of the recoil-ion energy spectra are not available. Here, a method which uses evenly-spaced fictitious excited states in the daughter nucleus to approximate the β-decay characteristics was developed to determine the detection efficiencies. The method can be used to constrain the decay properties using only data collected with the BPT detector array. For ^{137}I, the results from this method were compared to results from simulations based on nuclear data from both the NDS and MTAS, each in conjunction with γ-decay information from RIPL-3. The method was then applied to determine the detection efficiencies for other isotopes studied using the BPT.

Using this method, it is possible to determine the detector efficiency values for the BPT to within 4%, which paves the way for precisely determining β-delayed neutron branching ratios solely from the recoil-ion TOF spectra. Additionally, these results reveal that, with the exception of ^{137}I and ^{134}Sb, all isotopes studied have significant β-decay feeding to highly-excited states in the daughter nucleus that had not been previously identified.

Acknowledgments

This work was supported by the United States Department of Energy, Nuclear Energy University Program under Grant No. NEUP 13-5485 (University of California, Berkeley), by the United States Department of Energy, National Nuclear Security Administration under Grant No. DE-NA0000979 (National Nuclear Security Consortium), and Contract No. DE-AC52-07NA27344 (Lawrence Livermore National Laboratory), by the United States Department of Energy, Office of Science, Office of Nuclear Physics under Grant No. DE-FG02-94ER40834 (University of Maryland), Grant No. DE-FG02-98ER41086 (Northwestern University), and Contract No. DE-AC02-06CH11357 (Argonne National Laboratory), by the National Science Foundation under Grant PHY-1419765 (University of Notre Dame), by the Louisiana Board of Regents Research Competitiveness Subprogram under Award LEQSF(2016-19)-RD-A-09, and by the National Sciences and Engineering Research Council of Canada under Application Number 216974. This research used resources of ANL's ATLAS facility, which is a DOE Office of Science User Facility.

References

[1] D. Abriola, B. Singh, I. Dillmann, Summary report of consultants' meeting on beta-delayed neutron emission evaluation, Tech. rep., International Atomic Energy Agency (IAEA), iNDC(NDS)–0599, 2011.
[2] E. Kiefhaber, Influence of delayed neutron spectra on fast reactor criticality, Nucl. Sci. Eng. 111 (2) (1992) 197–204.
[3] R.J. Onega, R.J. Florian, The implication of sensitivity analysis on the safety and delayed-neutron parameters for fast breeder reactors, Ann. Nucl. Energy 10 (9) (1983) 477–490.
[4] K. Farouqi, K.-L. Kratz, B. Pfeiffer, T. Rauscher, F.-K. Thielemann, J.W. Truran, Charged-particle and neutron-capture processes in the high-entropy wind of core-collapse supernovae, Astrophys. J. 712 (2) (2010) 1359.
[5] R.M. Yee, N.D. Scielzo, P.F. Bertone, F. Buchinger, S. Caldwell, J.A. Clark, C.M. Deibel, J. Fallis, J.P. Greene, S. Gulick, D. Lascar, A.F. Levand, G. Li, E.B. Norman, M. Pedretti, G. Savard, R.E. Segel, K.S. Sharma, M.G. Sternberg, J. Van Schelt, B.J. Zabransky, β-delayed neutron spectroscopy using trapped radioactive ions, Phys. Rev. Lett. 110 (2013) 092501.
[6] S. Caldwell, A Trapped-Ion Technique for Beta-Delayed Neutron Studies (Ph.D. thesis), The University of Chicago, 2015.
[7] A. Czeszumska, β-delayed Neutron Studies of $^{137-138}$I and $^{144-145}$Cs Performed with Trapped Ions (Ph.D. thesis), University of California-Berkeley, 2016.
[8] N. Scielzo, G. Li, M. Sternberg, G. Savard, P. Bertone, F. Buchinger, S. Caldwell, J. Clark, J. Crawford, C. Deibel, J. Fallis, J. Greene, S. Gulick, A. Hecht, D. Lascar, J. Lee, A. Levand, M. Pedretti, R. Segel, H. Sharma, K. Sharma, I. Tanihata, J. Van Schelt, R. Yee, B. Zabransky, The Paul trap: A radiofrequency-quadrupole ion trap for precision studies, Nucl. Instrum. Methods Phys. Res. A 681 (2012) 94–100.
[9] J.L. Wiza, Microchannel plate detectors, Nucl. Instrum. Methods 162 (1) (1979) 587–601.
[10] E.K. Warburton, D.E. Alburger, D.H. Wilkinson, Electron-neutrino correlation in the first-forbidden beta decay of ^{11}Be, Phys. Rev. C 26 (1982) 1186–1197.
[11] K. Siegl, N.D. Scielzo, A. Czeszumska, G. Savard, A. Aprahamian, S.A. Caldwell, M. Burkey, C.J. Chiara, J.A. Clark, J.P. Greene, J. Harker, S.T. Marley, G.E. Morgan, J.M. Munson, E.B. Norman, R. Orford, S. Padgett, A. Perez Galvan, K.S. Sharma, S.Y. Strauss, Study of recoil ions from the β-decay of ^{134}Sb using the Beta-decay Paul Trap, Phys. Rev. C 97 (2018) 035504.
[12] G. Savard, S. Baker, C. Davids, A. Levand, E. Moore, R. Pardo, R. Vondrasek, B. Zabransky, G. Zinkann, Radioactive beams from gas catchers: The CARIBU facility, in: Proceedings of the XVth International Conference on Electromagnetic Isotope Separators and Techniques Related to their Applications, Nucl. Instrum. Methods Phys. Res. B 266 (19) (2008) 4086–4091.
[13] N.D. Scielzo, S.J. Freedman, B.K. Fujikawa, P.A. Vetter, Recoil-ion charge-state distribution following the β^+ decay of ^{21}Na, Phys. Rev. A 68 (2003) 022716.
[14] A. Sonzogni, Nuclear Data Sheets for A = 134, Nucl. Data Sheets 103 (1) (2004) 1–182.
[15] B. Singh, A.A. Rodionov, Y.L. Khazov, Nuclear Data Sheets for A = 135, Nucl. Data Sheets 109 (3) (2008) 517–698.
[16] A. Sonzogni, Nuclear Data Sheets for A = 136, Nucl. Data Sheets 95 (4) (2002) 837–994.
[17] E. Browne, J. Tuli, Nuclear Data Sheets for A = 137, Nucl. Data Sheets 108 (10) (2007) 2173–2318.
[18] A. Sonzogni, Nuclear Data Sheets for A = 138, Nucl. Data Sheets 98 (3) (2003) 515–664.
[19] N. Nica, Nuclear Data Sheets for A = 140, Nucl. Data Sheets 108 (7) (2007) 1287–1470.
[20] A. Sonzogni, Nuclear Data Sheets for A = 144, Nucl. Data Sheets 93 (3) (2001) 599–762.
[21] E. Browne, J. Tuli, Nuclear Data Sheets for A = 145, Nucl. Data Sheets 110 (3) (2009) 507–680.
[22] B.C. Rasco, K.P. Rykaczewski, A. Fijałkowska, M. Karny, M. Wolińska-Cichocka, R.K. Grzywacz, C.J. Gross, D.W. Stracener, E.F. Zganjar, J.C. Blackmon, N.T. Brewer, K.C. Goetz, J.W. Johnson, C.U. Jost, J.H. Hamilton, K. Miernik, M. Madurga, D. Miller, S. Padgett, S.V. Paulauskas, A.V. Ramayya, E.H. Spejewski, Complete β-decay pattern for the high-priority decay-heat isotopes ^{137}I and ^{137}Xe determined using total absorption spectroscopy, Phys. Rev. C 95 (2017) 054328.
[23] R. Capote, M. Herman, P. Obložinský, P. Young, S. Goriely, T. Belgya, A. Ignatyuk, A. Koning, S. Hilaire, V. Plujko, M. Avrigeanu, O. Bersillon, M. Chadwick, T. Fukahori, Z. Ge, Y. Han, S. Kailas, J. Kopecky, V. Maslov, G. Reffo, M. Sin, E. Soukhovitskii, P. Talou, RIPL - Reference Input Parameter Library for calculation of nuclear reactions and nuclear data evaluations, Nucl. Data Sheets 110 (12) (2009) 3107–3214.
[24] D. Manura, computer code SimIon 3D, version 80, Scientific Instrument Services, Inc., 2008.
[25] S. Agostinelli, J. Allison, K. Amako, J. Apostolakis, H. Araujo, P. Arce, M. Asai, D. Axen, S. Banerjee, G. Barrand, F. Behner, L. Bellagamba, J. Boudreau, L. Broglia, A. Brunengo, H. Burkhardt, S. Chauvie, J. Chuma, R. Chytracek, G. Cooperman, G. Cosmo, P. Degtyarenko, A. Dell'Acqua, G. Depaola, D. Dietrich, R. Enami, A. Feliciello, C. Ferguson, H. Fesefeldt, G. Folger, F. Foppiano, A. Forti, S. Garelli, S. Giani, R. Giannitrapani, D. Gibin, J.G. Cadenas, I. González, G.G. Abril, G. Greeniaus, W. Greiner, V. Grichine, A. Grossheim, S. Guatelli, P. Gumplinger, R. Hamatsu, K. Hashimoto, H. Hasui, A. Heikkinen, A. Howard, V. Ivanchenko, A. Johnson, F. Jones, J. Kallenbach, N. Kanaya, M. Kawabata, Y. Kawabata, M. Kawaguti, S. Kelner, P. Kent, A. Kimura, T. Kodama, R. Kokoulin, M. Kossov, H. Kurashige, E. Lamanna, T. Lampén, V. Lara, V. Lefebure, F. Lei, M. Liendl, W. Lockman, F. Longo, S. Magni, M. Maire, E. Medernach, K. Minamimoto, P.M. de Freitas, Y. Morita, K. Murakami, M. Nagamatu, R. Nartallo, P. Nieminen, T. Nishimura, K. Ohtsubo, M. Okamura, S. O'Neale, Y. Oohata, K. Paech, J. Perl, A. Pfeiffer, M. Pia, F. Ranjard, A. Rybin, S. Sadilov, E.D. Salvo, G. Santin, T. Sasaki, N. Savvas, Y. Sawada, S. Scherer, S. Sei, V. Sirotenko, D. Smith, N. Starkov, H. Stoecker, J. Sulkimo, M. Takahata, S. Tanaka, E. Tcherniaev, E.S. Tehrani, M. Tropeano, P. Truscott, H. Uno, L. Urban, P. Urban, M. Verderi, A. Walkden, W. Wander, H. Weber, J. Wellisch, T. Wenaus, D. Williams, D. Wright, T. Yamada, H. Yoshida, D. Zschiesche, Geant4—a simulation toolkit, Nucl. Instrum. Methods Phys. Res. A 506 (3) (2003) 250–303.
[26] J.D. Robertson, S.H. Faller, W.B. Walters, R.L. Gill, H. Mach, A. Piotrowski, E.F. Zganjar, H. Dejbakhsh, R.F. Petry, Decay of ^{145}Cs to levels of ^{145}Ba, Phys. Rev. C 34 (1986) 1012–1023.
[27] J. Hardy, L. Carraz, B. Jonson, P. Hansen, The essential decay of pandemonium: A demonstration of errors in complex beta-decay schemes, Phys. Lett. B 71 (2) (1977) 307–310.
[28] G. Rudstam, P. Johansson, O. Tengblad, P. Aagaard, J. Eriksen, Beta and gama spectra of short-lived fission products, At. Data Nucl. Data Tables 45 (2) (1990) 239–320.
[29] S.G. Prussin, Nuclear Physics for Applications, A Model Approach, Wiley-VCH Verlag GmbH & Co, Weinheim, 2007.